Bonn potential and shell-model calculations for $N=126$ isotones

L. Coraggio,[1,2] A. Covello,[1] A. Gargano,[1] N. Itaco,[1] and T. T. S. Kuo[2]
[1]*Dipartimento di Scienze Fisiche, Università di Napoli Federico II, and Istituto Nazionale di Fisica Nucleare, Complesso Universitario di Monte S. Angelo, Via Cintia, I-80126 Napoli, Italy*
[2]*Department of Physics, State University of New York at Stony Brook, Stony Brook, New York 11794*
(Received 6 July 1999; published 5 November 1999)

We have performed shell-model calculations for the $N=126$ isotones ^{210}Po, ^{211}At, and ^{212}Rn using a realistic effective interaction derived from the Bonn-A nucleon-nucleon potential by means of a *G*-matrix folded-diagram method. The calculated binding energies, energy spectra, and electromagnetic properties show remarkably good agreement with the experimental data. The results of this paper complement those of our previous study on neutron hole Pb isotopes, confirming that realistic effective interactions are now able to reproduce with quantitative accuracy the spectroscopic properties of complex nuclei.
[S0556-2813(99)02611-4]

PACS number(s): 21.60.Cs, 21.30.Fe, 27.80.+w

I. INTRODUCTION

During the past few years, we have studied a number of nuclei around doubly magic ^{100}Sn and ^{132}Sn [1–5] in terms of the shell model employing realistic effective interactions derived from the meson-theoretic Bonn-A nucleon-nucleon (*NN*) potential [6]. In these studies we have considered nuclei with few valence particles or holes, their properties being of special interest for a stringent test of the basic ingredients of shell-model calculations. The aim of our work is to assess the ability of realistic effective interactions to provide a quantitative description of nuclear structure properties. This is in fact a key point to understand if the time has come to make the shell model a truly microscopic theory of nuclear structure.

As is well known, the first step in this direction was taken more than 30 years ago by Kuo and Brown [7] who derived an *sd*-shell effective interaction from the Hamada-Johnston potential [8]. Later on, an effective interaction for the lead region was derived [9] by Kuo and Herling (KH) from the same potential. Since then, however, substantial progress has been made in both the development of high-quality *NN* potentials and the many-body methods for calculating the matrix elements of the effective interaction.

As regards the first point, modern potentials reproduce quite accurately all the known *NN* scattering data. A review of recent developments in the field of *NN* potentials is given in Refs. [10,11]. We only recall here that two potentials which fit equally well the *NN* data up to the inelastic threshold may differ substantially in their off-shell behavior. Thus, different *NN* potentials may produce somewhat different nuclear structure results.

As for the second point, an accurate calculation of the Brueckner *G* matrix is now feasible while the so-called folded-diagram expansion yields a rigorous expression for the model-space effective interaction $V_{\rm eff}$. The main aspects of the above derivation of $V_{\rm eff}$ are described in Refs. [12,13].

Based on these improvements, a new generation of realistic effective interactions has become available, fostering renewed interest in realistic shell-model calculations. It is in this context that our recent studies of medium-mass nuclei are framed. The remarkably good agreement between theory and experiment obtained for these nuclei has challenged us to perform the same kind of realistic shell-model calculations for heavy-mass nuclei. In a previous work [14] we considered the neutron hole isotopes ^{206,205,204}Pb. Here, we present the results of a companion study of the $N=126$ isotones, focusing attention on ^{210}Po, ^{211}At, and ^{212}Rn. These nuclei, with two to four protons in the $Z=82-126$ shell, offer the opportunity to further test our realistic effective interactions in the lead region.

The $N=126$ nuclei, as well as the lead isotopes, have long been the subject of both experimental and theoretical studies. From the experimental point of view, these stable or near-stable nuclei have been extensively investigated and a rather large amount of experimental data is available for them. On the other hand, the good doubly magic character of ^{208}Pb has motivated many shell-model calculations in this region. In all the calculations performed so far, however, phenomenological interactions have been used [15,16], the only notable exception being the pioneering work of McGrory and Kuo [17], where the KH interaction was employed.

The outline of the paper is as follows. In Sec. II we give an outline of our calculations, including a brief review of the derivation of the effective interaction. In Sec. III we present the results obtained for binding energies, energy spectra and electromagnetic properties, comparing them with the experimental data. Section IV contains a discussion and a summary of our conclusions.

II. OUTLINE OF CALCULATIONS

We assume that ^{208}Pb is a closed core and let the valence protons occupy the six single-particle (SP) orbits $0h_{9/2}$, $1f_{7/2}$, $0i_{13/2}$, $1f_{5/2}$, $2p_{3/2}$, and $2p_{1/2}$. We take the SP energies from the experimental spectrum of ^{209}Bi [18]. They are (in MeV): $\epsilon_{h_{9/2}}=0.0$, $\epsilon_{f_{7/2}}=0.896$, $\epsilon_{i_{13/2}}=1.609$, $\epsilon_{f_{5/2}}=2.826$, $\epsilon_{p_{3/2}}=3.119$, $\epsilon_{p_{1/2}}=3.633$.

As already mentioned in the Introduction, we use in the present calculation a realistic effective interaction derived from the Bonn-A free *NN* potential. Let us now outline our

derivation of $V_{\rm eff}$. Because of the strong repulsive core contained in the Bonn-A potential, which is a feature common to all modern NN potentials, the model-space G matrix corresponding to the chosen V_{NN} must be calculated first. The G matrix is defined [19] by the integral equation

$$G(\omega)=V+VQ_2\frac{1}{\omega-Q_2TQ_2}Q_2G(\omega), \tag{1}$$

where V represents the NN potential, T denotes the two-nucleon kinetic energy, and ω is an energy variable (the so-called starting energy). The two-body Pauli exclusion operator Q_2 prevents double counting, namely, the intermediate states allowed for G must be outside of the chosen model space. Thus the Pauli operator Q_2 is dependent on the model space, and so is the G matrix. The operator Q_2 is specified, as discussed in Ref. [19], by a set of three numbers (n_1,n_2,n_3) each representing a shell-model orbital (we number the orbits starting from the bottom of the oscillator well; for instance, the orbit $0d_{5/2}$ is denoted as orbit 4 and $0h_{11/2}$ as orbit 16). Note that in Eq. (1) the Pauli exclusion operator Q_2 is defined in terms of harmonic oscillator wave functions while plane-wave functions are employed for the intermediate states of the G matrix.

Since the valence-proton and -neutron orbits outside ^{208}Pb are different, our Q_2 operators for protons and for neutrons are different and consequently our G-matrix calculation is considerably more complicated than in the case when the two operators are the same. In the present calculation we have fixed $(n_1,n_2,n_3)=(22,45,78)$ for the neutron orbits, and $(n_1,n_2,n_3)=(16,36,78)$ for the proton orbits. Our procedure for calculating the G matrix is outlined below. We first calculate the free G matrix G_F in a proton-neutron representation, G_F being defined by

$$G_F=V+V\frac{1}{e}G_F, \tag{2}$$

with $e\equiv(\omega-T)$. Note that G_F does not contain the Pauli exclusion operator and hence its calculation is relatively convenient. Then we calculate the Pauli correction term [19,20],

$$\Delta G=-G_F\frac{1}{e}P_2\frac{1}{P_2[1/e+(1/e)G_F(1/e)]P_2}P_2\frac{1}{e}G_F, \tag{3}$$

where $P_2=1-Q_2$, separately for protons and for neutrons. Finally the full G matrix as defined by Eq. (1) is obtained as

$$G=G_F+\Delta G. \tag{4}$$

For the harmonic oscillator parameter $\hbar\omega$ we use the value 6.88 MeV, as obtained from the expression $\hbar\omega=45A^{-1/3}-25A^{-2/3}$ for $A=208$. Note that in the present work we have chosen the value of n_2 so as to include three harmonic oscillator shells above the Fermi level denoted by n_1. In earlier works on light- and medium-mass nuclei, n_2 was fixed by taking into account only two major shells above the n_1-th orbit. For instance, a common choice for sd-shell calculations is $n_2=10$ with $n_1=3$ [12]. For the $N=126$ isotones, however, the present choice is more appropriate. In fact, these calculations as well as those for lead isotopes [14,21] have led to a substantially better agreement with experiment when in the derivation of the effective interaction n_2 has been increased from two to three shells above the n_1-th orbit.

Using the above G matrix we then calculate the irreducible vertex function $\hat{Q}$ box, which is composed of irreducible valence-linked G-matrix diagrams through second order in G. These are precisely the seven first- and second-order diagrams considered by Shurpin *et al.* [22]. The effective interaction can be written in operator form as

$$V_{\rm eff}=\hat{Q}-\hat{Q}'\int\hat{Q}+\hat{Q}'\int\hat{Q}\int\hat{Q}-\hat{Q}'\int\hat{Q}\int\hat{Q}\int\hat{Q}+\cdots, \tag{5}$$

where $\hat{Q}$ is the $\hat{Q}$ box, and the integral sign represents a generalized folding operation [23]. $\hat{Q}'$ is obtained from $\hat{Q}$ by removing terms of first order in the reaction matrix G. After the $\hat{Q}$ box is calculated, the energy-independent $V_{\rm eff}$ is then obtained by summing up the folded-diagram series of Eq. (5) to all orders using the Lee-Suzuki iteration method [24]. This last step can be performed in an essentially exact way for a given $\hat{Q}$ box. Once the effective interaction has been derived, the shell-model calculations are carried out employing the OXBASH code [25].

As regards the electromagnetic observables, we have calculated them by making use of effective operators [26,27] which take into account core-polarization effects. More precisely, by using a diagrammatic description as in Ref. [26], we have only included first-order diagrams in G. This implies that folded-diagram renormalizations are not necessary [27].

As is well known, the nuclear magnetic properties may be significantly affected by mesonic exchange currents. An estimate of their contribution for nuclei in the vicinity of ^{208}Pb has been given in Refs. [28,29]. This amounts to renormalizing the gyromagnetic factor g_l from the bare value of $g_l=1$ to 1.155 and g_s from 5.586 to 5.699. We have made use of these values in our calculation of the effective $M1$ operator.

III. RESULTS AND COMPARISON WITH EXPERIMENT

In this section the results of our calculations for the three nuclei ^{210}Po, ^{211}At, and ^{212}Rn are presented and compared with experiment. The energy spectra are presented separately for each isotone in the three following subsections. For ^{210}Po a detailed comparison between calculated and observed spectroscopic factors is also reported. The last subsection is devoted to the discussion of the electromagnetic properties of all three nuclei.

The calculated ground-state binding energies relative to ^{208}Pb are compared with the observed values [30] in Table I. The mass excess value for ^{209}Bi needed for absolute scaling of the SP levels was taken from Ref. [30]. As regards the Coulomb interaction between the valence protons, we have

TABLE I. Experimental and calculated ground-state binding energies (MeV) relative to ^{208}Pb for ^{210}Po, ^{211}At, and ^{212}Rn.

Nucleus	Binding energy	
	Expt.	Calc.
^{210}Po	8.782 ± 0.004	8.789
^{211}At	11.765 ± 0.005	11.816
^{212}Rn	16.065 ± 0.006	16.146

assumed that it gives a contribution proportional to the number of interacting proton pairs, namely, $E_C = [n(n-1)/2]V_C$ (n is the number of valence protons). The strength V_C has been taken to be 270 keV, which is the value of the matrix element of the Coulomb force between two $h_{9/2}$ protons with $J=0$.

From Table I we see that a very good agreement with experiment is obtained for all three nuclei. In fact, the calculated binding energy for ^{210}Po falls practically within the error bar, while the other two calculated values differ by less than 100 keV from the experimental ones.

A. Spectrum of ^{210}Po

The experimental [18] and theoretical spectra of ^{210}Po are compared in Fig. 1. Here all the calculated and experimental levels up to 3.3 MeV are reported, while in the higher-energy region the negative-parity states have been excluded (in this energy region we have also omitted three experimental states without spin and parity assignment). The calculated states which are shown in Fig. 1 are all the 44 states arising from the configurations $h^2_{9/2}$, $h_{9/2}f_{7/2}$, $h_{9/2}i_{13/2}$, $f^2_{7/2}$, $i^2_{13/2}$, $h_{9/2}f_{5/2}$, and $h_{9/2}p_{3/2}$. In the energy region 3.5–4.5 MeV we find the eight negative-parity states of the $f_{7/2}i_{13/2}$ configuration, but for them, as mentioned above, we have not tried to establish any correspondence with observed levels. In fact, in this energy interval negative-parity states have been observed which cannot be described within our model space. As an example, we mention the 12^- and 13^- states, which cannot be constructed in our model space, and the three 5^- levels observed at 3.43, 3.70, and 3.71 MeV to which corresponds only one calculated 5^- state at 3.85 MeV. These experimental ''extra'' levels arise from core excitations, and in some cases significant admixtures of these excitations and two-particle model-space states are likely to occur.

In Fig. 1 we see that the calculated spectrum is characterized by four groups of levels: the first one up to 1.6 MeV, the second between 2.2 and 2.5 MeV, the third between 2.7 and 3.3 MeV, and the fourth above 3.8 MeV. The five levels of the first group are dominated by the $h^2_{9/2}$ configuration, while the second group contains all the members of the $h_{9/2}f_{7/2}$ multiplet, in addition to the 0^+ state arising from the $f^2_{7/2}$ configuration. The other three states of this latter configuration together with all the states arising from the $h_{9/2}i_{13/2}$ configuration are in the third group. All the states in these three groups, with few exceptions, are almost pure, the percentage of the dominant configuration ranging from 95 to 100 %. Only for the ground state and the 0^+_2 and 2^+_3 states the contribution coming from configurations other than the dominant one is particularly significant, the percentage of such configurations being 21, 28, and 16 %, respectively. The 17 levels arising from the configurations $i^2_{13/2}$, $h_{9/2}f_{5/2}$, and $h_{9/2}p_{3/2}$ all lie in the energy interval 3.8–4.8 MeV. It should be mentioned, however, that for most of these states the wave functions are not quite pure. In particular, we find that a significant admixture of the three above configurations is present in the even J states.

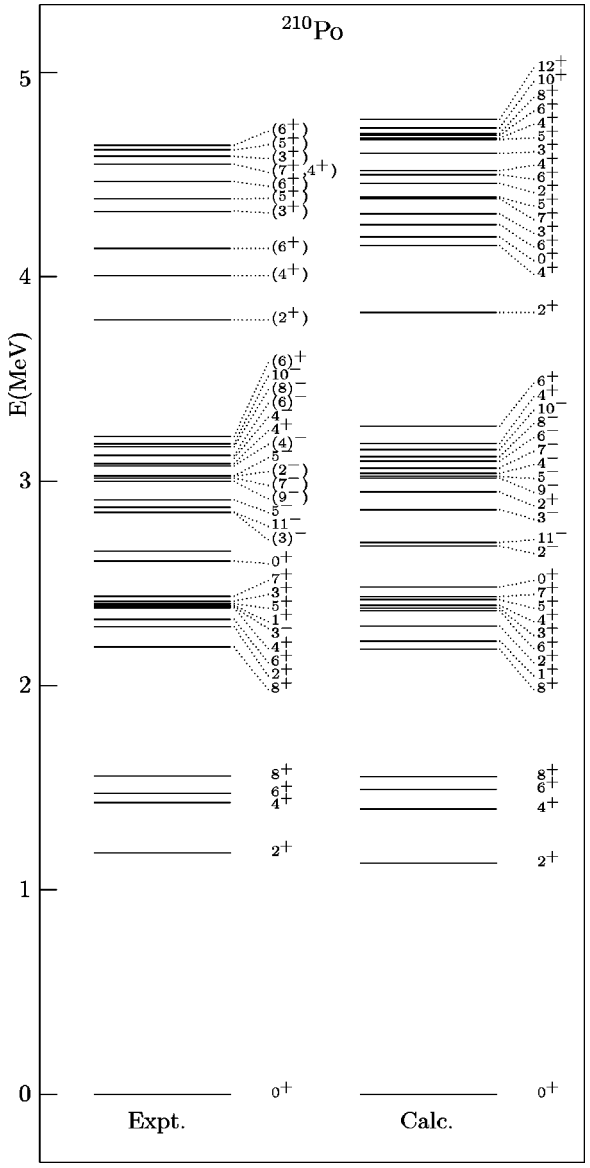

FIG. 1. Experimental and calculated spectrum of ^{210}Po.

Up to 3.3 MeV excitation energy each state of a given J^π in the calculated spectrum can be unambiguously associated with an observed level, the only exception being the 2^+_3 state at 2.95 MeV excitation energy. However, two levels with no angular momentum and parity assignment have been observed at 2.66 and 2.87 MeV, and in Ref. [31] it is suggested that the 2.87-keV γ ray measured in the ^{209}Bi$(t,2n)^{210}$Po reaction is a good candidate for the $2^+_3 \rightarrow 0^+_{gs}$ transition. The experimental 3^-_1 state at 2.39 MeV, as well as the the 5^-_1 and

4_2^- states at 2.91 and 3.11 MeV, respectively, have no theoretical counterpart. In fact, the first one reflects the collective nature of the octupole 3^- state at 2.61 MeV in ^{208}Pb, while the other two levels arise from the neutron particle-hole configuration $\nu(g_{9/2}p_{1/2}^{-1})$ [31], and therefore cannot be described within our model space. It should be noted that each of the two above 5_1^- and 4_2^- levels lies very close in energy to the state with the same J^π originating from the $h_{9/2}i_{13/2}$ configuration. Therefore it cannot be excluded, as we shall see when discussing the spectroscopic factors, that some mixing occurs between single-particle and core-excited states.

Above 3.8 MeV only 10 out of the 17 levels arising from the configurations $i_{13/2}^2$, $h_{9/2}f_{5/2}$, and $h_{9/2}p_{3/2}$ have been experimentally identified. For all of them, except the $(7^+,4^+)$ state at 4.55 MeV, a correspondence with states predicted by the theory can be safely established. As for the $(7^+,4^+)$ state, it may be associated with either the 7_2^+ or the 4_5^+ calculated states, which lie at 4.48 and 4.52 MeV excitation energy, respectively. In a very recent work [32] the assignment 7^+ has been proposed for the experimental level at 4.55 MeV and a new level with $J^\pi=(4^+)$ has been identified at 4.54 MeV.

As regards the quantitative agreement, we see from Fig. 1 that it is very satisfactory, the discrepancies between calculated and experimental excitation energies being less than 100 keV for most of the states. More precisely, including the level at 2.87 MeV (identified as a $J^\pi=2^+$ state) as well as the $J^\pi=4^+$ and 7^+ of Ref. [32], 37 observed levels have been associated with states predicted by the theory, and only for seven of them the experimental and calculated excitation energies differ by more than 100 keV. The rms deviation σ [33] relative to these 37 levels is 87 keV.

In Ref. [34] the ^{209}Bi(^{3}He,d)^{210}Po and ^{209}Bi(^{4}He,t)^{210}Po reactions have been studied and the single-proton strengths of transitions to various excited levels in ^{210}Po have been extracted from the measured cross sections. These observed strengths are compared with the calculated values in Table II, where we also list the experimental and theoretical excitation energies. The experimental uncertainties appearing in Table II are only statistical and the numbers in parentheses, which correspond to levels not fully resolved, were extracted by a peak fitting procedure (see Ref. [34]). The theoretical spectroscopic factor S is defined as

$$S_{l_j}^{J^\pi\beta}=\frac{1}{2J+1}|\langle^{210}\mathrm{Po},\, J^\pi,\, \beta\|a_{lj}^\dagger\|^{209}\mathrm{Bi},\, J_i^\pi=9/2^-,\, \mathrm{g.s.}\rangle|^2,$$

where we assume that the ground state of ^{209}Bi is a single $h_{9/2}$ proton outside the doubly magic ^{208}Pb. The label β specifies states of ^{210}Po with the same J^π.

From Table II we see that for almost all the states of the three low-lying multiplets the agreement between theory and experiment is very good. Actually, a significant discrepancy exists only for the 11^- state and the 5^- state at 3.02 MeV. However, it was suggested in Ref. [34] that the level at 2.85 MeV was an unresolved doublet with $J^\pi=11^-$ and 3^-, as it has been found later to be the case [18]. Thus the observed strength 3.25 attributed to the 11^- state has to be compared to the sum of the two calculated strengths relative to the 11^- and 3^- states, which are 2.30 and 0.69, respectively. As for the 5^- state, our calculation overestimates the experimental value. Part of the single particle strength is contained in the first 5^- state, which, as mentioned above, is not predicted by the theory, being essentially a core-excited state.

In the region above 3.8 MeV the values of the measured strengths ($l=1$ and 3) are generally smaller than those relative to the states of the three low-lying multiplets. On the other hand, as it was already pointed out at the beginning of this section, the calculated wave functions of several states in this region show a strong admixture of the configurations $i_{13/2}^2$, $h_{9/2}f_{5/2}$, and $h_{9/2}p_{3/2}$. Thus, a comparison between theory and experiment may provide a test of the calculated percentages of the $h_{9/2}f_{5/2}$ and $h_{9/2}p_{3/2}$ configurations (obviously, the contribution of the $i_{13/2}^2$ configuration is not determined directly from the measured strengths). It should also be noted that the experimental data do not allow to distinguish between $p_{3/2}$ and $p_{1/2}$ transfers. We have found, however, that a small component of the $h_{9/2}p_{1/2}$ configuration is present only in the two 4^+ states at 4.15 and 4.55 MeV, respectively. From Table II we see to the observed strengths of the states above 3.8 MeV are quite well reproduced by the theory. Note that the level at 4.55 MeV excited via $f_{5/2}$ transfer is likely to correspond to an unresolved doublet with $J^\pi=4^+$ and 7^+ (see discussion above). In this case the measured strength, 1.83, should be interpreted as the sum of the calculated strengths 1.50 and 0.20 relative to the 7^+ and 4^+ states at 4.38 and 4.55 MeV, respectively. In this connection, it should be pointed out that the observed strength of the level at 4.55 MeV excited via $l=1$ transfer and assigned $J^\pi=4^+$ [34] is also well reproduced by our calculation.

B. Spectrum of ^{211}At

The experimental [18] and theoretical spectra of ^{211}At are compared in Fig. 2, where all the observed levels up to 3.3 MeV excitation energy are reported. In the calculated spectrum all the levels up to about 2.0 MeV are included while in the higher-energy region only the states which can be associated to the observed ones are reported. For the sake of completeness all the calculated excitation energies up to 2.7 MeV are listed in Table III.

From Fig. 2 we see that a one-to-one correspondence can be established between the experimental and calculated levels up to 1.5 MeV, the only exception being the experimental $(\frac{9}{2},\frac{11}{2},\frac{13}{2})$ level at 1.35 MeV which can be associated to either the $(\frac{9}{2}^-)_2$ or $(\frac{13}{2}^+)_1$ calculated state. As regards the two observed levels with no firm spin assignment at 1.12 and 1.23 MeV, we propose the assignment $J^\pi=\frac{11}{2}^-$ and $\frac{15}{2}^-$, respectively.

Above 1.5 MeV many more levels than the experimental ones are predicted by our calculations (see Table III). In particular, in the energy interval 1.5–2.0 MeV only three levels have been observed. These three states have $J^\pi=(\frac{3}{2})^-$, $(\frac{23}{2}^-)$, and $(\frac{5}{2})^-$ and can be identified with the calculated states with the same angular momentum and parity at 1.82, 1.97, and 2.04 MeV, respectively. It should be

TABLE II. Comparison of the experimentally observed spectroscopic strengths from the ^{209}Bi$(\alpha,t)^{210}$Po and ^{209}Bi$(^3$He$,d)^{210}$Po reactions with the calculated values. See text for comments.

l_j	J^π	$E_{\rm exp}$(MeV)	$E_{\rm calc}$(MeV)	$\frac{(2J+1)}{(2J_i+1)}S(\alpha,t)$	$\frac{(2J+1)}{(2J_i+1)}S(^3He,d)$	Calc.
$h_{9/2}$	2^+	1.181	1.130	1.00±0.06	1.16±0.22	0.98
	4^+	1.427	1.395	1.79±0.07	1.58±0.28	1.78
	6^+	1.473	1.493	2.64±0.09	2.63±0.25	2.58
	8^+	1.557	1.555	3.40±0.11	3.42±0.26	3.36
$f_{7/2}$	8^+	2.188	2.179	1.71±0.03	1.64±0.05	1.68
	2^+	2.290	2.292	0.42±0.01	0.42±0.02	0.47
	6^+	2.326	2.367	1.31±0.03	1.26±0.04	1.28
	4^+	2.382	2.394	(0.90)	(0.90)	0.88
	1^+	2.393	2.220	(0.31)	(0.35)	0.30
	5^+	2.403	2.422	(1.10)	(1.10)	1.10
	3^+	2.414	2.380	(0.72)	(0.75)	0.70
	7^+	2.438	2.437	1.51±0.03	1.50±0.06	1.50
$i_{13/2}$	3^-	2.846	2.862			0.69
	11^-	2.849	2.700	3.25±0.06		2.30
	5^-	2.910		0.31±0.01		
	9^-	2.999	3.016	(1.88)		1.89
	7^-	3.016	3.065	(1.53)		1.50
	2^-	3.024	2.682	(0.54)		0.50
	5^-	3.026	3.024	(0.78)		1.10
	4^-	3.075	3.039	0.78±0.02		0.90
	6^-	3.125	3.097	(1.34)		1.30
	8^-	3.168	3.121	(1.66)		1.70
	10^-	3.183	3.154	2.11±0.04		2.10
$f_{5/2}$	2^+	3.792	3.828	0.35±0.02		0.34
	4^+	4.027	4.152	0.60		0.67
	6^+	4.139	4.256	0.82		0.86
	3^+	4.320	4.309	0.86±0.04		0.69
	5^+	4.382	4.391	1.19±0.05		1.10
	6^+	4.469	4.503	0.55±0.03		0.43
	7^+,4^+	4.553	4.384,4.552	1.83±0.07		1.50,0.20
$p_{3/2}+p_{1/2}$	4^+	4.027	4.152		0.03	0.07
	6^+	4.139	4.256		0.20	0.29
	6^+	4.469	4.503		0.56±0.04	0.66
	4^+	4.553	4.522		0.35±0.07	0.22
	3^+	4.591	4.605		(0.75)	0.69
	5^+	4.624	4.673		(1.35)	1.10
	6^+	4.644	4.691		(0.55)	0.31

noted that we predict the existence of a lower-lying $\frac{5}{2}^-$ state at 1.85 MeV.

As regards the states above 2.0 MeV, we identify the experimental $J^\pi=\frac{1}{2}^-,\frac{3}{2}^-$ level at 2.06 MeV with the calculated one with $J^\pi=\frac{1}{2}^-$ at 2.11 MeV, thus confirming the tentative assignment of Ref. [35]. As far as the lowest $\frac{1}{2}^+$ state is concerned, the calculated energy is 2.78 MeV, namely, 300 keV higher than that of the observed one. However, this state, which was populated in a first-forbidden β^+ decay of the ground state of ^{211}Rn [35], has been interpreted as a core-excited $^{212}\mathrm{Rn}\otimes(\pi s_{1/2})^{-1}$ state and, as such, is not expected to be adequately reproduced within our model space. In Ref. [35] the nature and assignment of the $J=\frac{1}{2},\frac{3}{2}$ level at 2.65 MeV was also discussed, but no definite conclusion was reached. We may only mention here that up to 3.5 MeV our calculations predict the existence of the three $\frac{3}{2}^+$ states reported in Fig. 2 and of no other $\frac{1}{2}^+$ aside from the above-mentioned one.

The quantitative agreement between our results and experiment is very satisfactory. In fact, the discrepancies for the excitation energies are all in the order of few tens of keV, the only exception being the $J^\pi=\frac{29}{2}^+$ state, which comes about 170 keV below its experimental counterpart. Excluding the $\frac{1}{2}^+$ state and the two levels at 1.35 and 2.65 MeV, for which we have not attempted any identification, the σ value is only 64 keV.

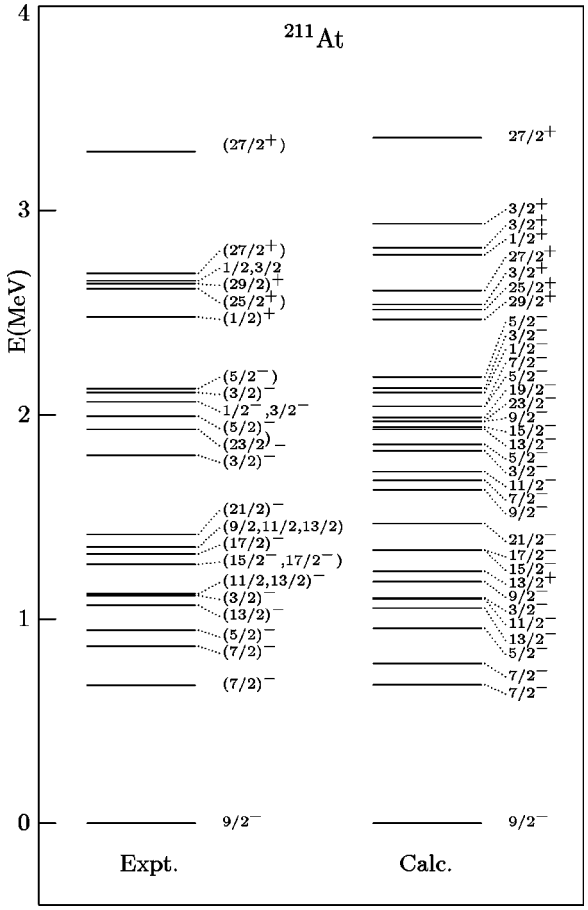

FIG. 2. Experimental and calculated spectrum of ^{211}At.

It should be noted that all the ten levels arising from the $h^3_{9/2}$ configuration lie at an excitation energy smaller than 1.5 MeV. In this energy region we also find the two seniority $v=1$ states of the $h^2_{9/2}f_{7/2}$ and $h^2_{9/2}i_{13/2}$ configurations. The latter states as well as the ground state contain, however, significant configuration mixing. In fact, the percentage of configurations other than the dominant one is 22% in the ground and $(\frac{7}{2}^-)_1$ states, reducing to 14% in the $(\frac{13}{2}^+)_1$ state. In all other levels up to 1.5 MeV the percentage of the dominant configuration ranges from 90–98 %. Above 1.5 MeV the negative-parity states are members of the multiplet $h^2_{9/2}f_{7/2}$, while all the positive-parity ones originate from the $h^2_{9/2}i_{13/2}$ configuration, except the $(\frac{27}{2}^+)_2$ state, which arises from the $h_{9/2}f_{7/2}i_{13/2}$ configuration. All these states are essentially pure, the only exception being the $(\frac{9}{2}^-)_4$ state, which contains 38% of the $h_{9/2}f^2_{7/2}$ configuration.

C. Spectrum of ^{212}Rn

Rather little experimental information [18] is presently available for ^{212}Rn. Up to about 4 MeV only 22 excited states have been identified (nine of them with unknown spin and parity), while our calculations predict a much higher level density. In particular, in the low-energy region (up to 2.5 MeV) we find 21 excited states compared to 7 in the experimental spectrum (two of them without spin-parity assignment). In this situation, any attempt to associate calculated states with experimental levels without assigned spin and parity may be misleading. Therefore, in Fig. 3 we exclude such states in the experimental spectrum and report only those yrast and yrare calculated states which are candidates for the observed levels. For completeness, all the calculated excitation energies up to about 2.6 MeV are listed in Table IV. It should be mentioned that above 4 MeV excitation energy several high-spin states have been observed. In Fig. 3, however, we do not include these levels, since their description is likely to require that core-excited states be explicitly taken into account.

From Fig. 3 we see that the calculated spectrum reproduces very well the experimental one, the discrepancies being smaller than 100 keV for the energies of 9 out of the 13 states considered. The rms deviation σ is only 85 keV, in line with the values obtained for the two lighter isotones.

As regards the structure of the states, we find that the wave functions of the seven higher-lying levels are substantially pure. These states are members of the three multiplets

TABLE III. Calculated low-energy levels of ^{211}At.

J^π	E(MeV)	J^π	E(MeV)	J^π	E(MeV)
$\frac{9}{2}^-$	0.0	$\frac{5}{2}^-$	2.040	$\frac{19}{2}^-$	2.350
$\frac{7}{2}^-$	0.679	$\frac{7}{2}^-$	2.042	$\frac{9}{2}^+$	2.393
$\frac{7}{2}^-$	0.783	$\frac{11}{2}^-$	2.042	$\frac{11}{2}^+$	2.412
$\frac{5}{2}^-$	0.955	$\frac{17}{2}^-$	2.045	$\frac{19}{2}^+$	2.427
$\frac{13}{2}^-$	1.053	$\frac{9}{2}^-$	2.080	$\frac{29}{2}^+$	2.466
$\frac{11}{2}^-$	1.098	$\frac{11}{2}^-$	2.110	$\frac{21}{2}^+$	2.472
$\frac{3}{2}^-$	1.103	$\frac{1}{2}^-$	2.110	$\frac{25}{2}^+$	2.515
$\frac{9}{2}^-$	1.186	$\frac{15}{2}^+$	2.124	$\frac{23}{2}^+$	2.528
$\frac{13}{2}^+$	1.236	$\frac{3}{2}^-$	2.131	$\frac{11}{2}^+$	2.530
$\frac{15}{2}^-$	1.337	$\frac{13}{2}^+$	2.136	$\frac{7}{2}^+$	2.539
$\frac{17}{2}^-$	1.339	$\frac{21}{2}^-$	2.178	$\frac{3}{2}^+$	2.541
$\frac{21}{2}^-$	1.467	$\frac{7}{2}^-$	2.181	$\frac{5}{2}^+$	2.549
$\frac{9}{2}^-$	1.631	$\frac{5}{2}^-$	2.185	$\frac{11}{2}^-$	2.560
$\frac{7}{2}^-$	1.681	$\frac{9}{2}^-$	2.189	$\frac{9}{2}^+$	2.574
$\frac{11}{2}^-$	1.721	$\frac{13}{2}^-$	2.204	$\frac{13}{2}^+$	2.589
$\frac{3}{2}^-$	1.824	$\frac{9}{2}^-$	2.229	$\frac{27}{2}^+$	2.609
$\frac{5}{2}^-$	1.856	$\frac{11}{2}^-$	2.238	$\frac{5}{2}^-$	2.617
$\frac{13}{2}^-$	1.929	$\frac{15}{2}^-$	2.245	$\frac{13}{2}^-$	2.625
$\frac{15}{2}^-$	1.940	$\frac{17}{2}^+$	2.279	$\frac{17}{2}^+$	2.629
$\frac{9}{2}^-$	1.967	$\frac{13}{2}^-$	2.282	$\frac{9}{2}^-$	2.686
$\frac{23}{2}^-$	1.969	$\frac{17}{2}^-$	2.289	$\frac{9}{2}^+$	2.688
$\frac{19}{2}^-$	1.987	$\frac{15}{2}^-$	2.291		

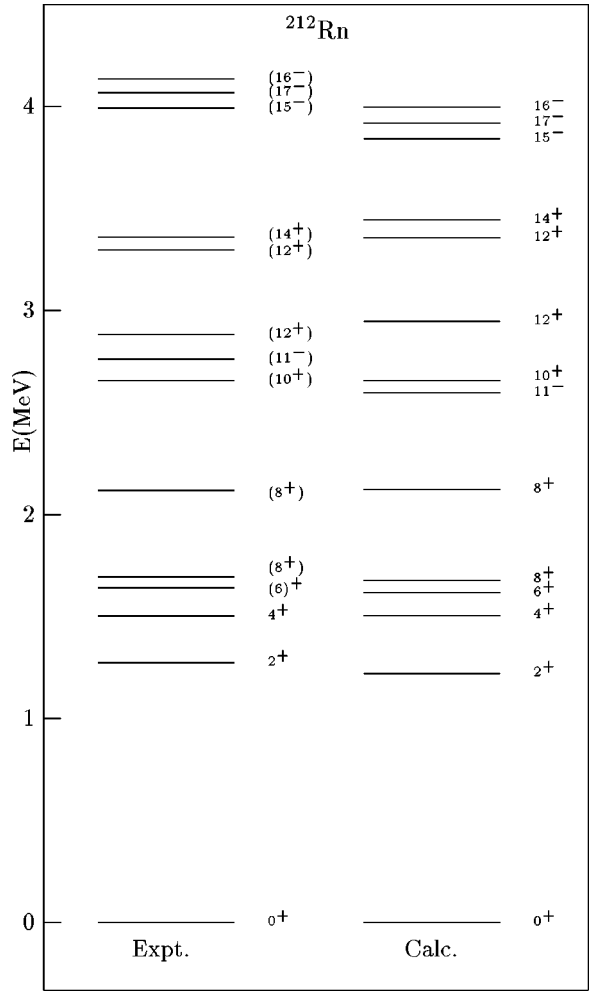

FIG. 3. Experimental and calculated spectrum of ^{212}Rn.

$h^4_{9/2}$ ($J^\pi = 10^+, 12^+_1$), $h^3_{9/2}f_{7/2}$ ($J^\pi = 12^+_2, 14^+$), and $h^3_{9/2}i_{13/2}$ ($J^\pi = 15^-, 16^-, 17^-$), and the percentage of the dominant configuration is at least 95%. This is not the case for the lower-lying states, whose wave functions contain significant configuration mixing. In the first four excited states the percentage of the dominant configuration, $h^4_{9/2}$, ranges from 71 to 76 % while it becomes 55% in the ground state. As for the 8^+_2 and 11^- states, the percentages of the dominant configurations, $h^3_{9/2}f_{7/2}$ and $h^3_{9/2}i_{13/2}$, are 80 and 82 %, respectively.

TABLE IV. Calculated low-energy levels of ^{212}Rn.

J^π	E(MeV)	J^π	E(MeV)
0^+	0.0	3^+	2.276
2^+	1.221	4^+	2.277
4^+	1.506	5^+	2.290
6^+	1.619	5^+	2.357
8^+	1.677	7^+	2.387
4^+	2.057	4^+	2.450
8^+	2.122	3^+	2.473
0^+	2.170	0^+	2.499
6^+	2.177	6^+	2.561
2^+	2.198	2^+	2.581
1^+	2.208	11^-	2.597
2^+	2.211	8^+	2.632
6^+	2.226	3^-	2.651
7^+	2.274	10^+	2.655

TABLE V. Calculated and experimental dipole moments (in nm).

Nucleus	J^π	μ	
		Calc.	Expt.
^{210}Po	6^+_1	+5.29	$\pm$5.48$\pm$0.05
	8^+_1	+7.06	+7.35$\pm$0.05
	11^-_1	+13.12	+12.20$\pm$0.09
^{211}At	$(\frac{15}{2}^-)_1$	+6.6	$\pm$6.8$\pm$0.6
	$(\frac{21}{2}^-)_1$	+9.32	+9.56$\pm$0.09
	$(\frac{29}{2}^+)_1$	+16.23	+15.31$\pm$0.13
^{212}Rn	4^+_1	+3.56	$\pm$4.04$\pm$0.24
	6^+_1	+5.308	$\pm$5.454$\pm$0.048
	8^+_1	+7.064	+7.152$\pm$0.016
	14^+_1	+15.07	$\pm$14.98$\pm$0.42
	17^-_1	+18.45	$\pm$17.85$\pm$0.17

D. Electromagnetic properties

The effective operators needed for the calculation of electromagnetic observables have been derived as described in Sec. II. In Table V we compare the experimental magnetic moments in ^{210}Po, ^{211}At, and ^{212}Rn [18,36] with the calculated values. We see that the agreement is remarkably good in all cases. Only two $M1$ reduced transition probabilities are known in ^{211}At [18,37]. They are compared with our theoretical results in Table VII. We see that both the calculated and experimental values are extremely small.

Let us now come to the electric observables. In Tables VI and VII we compare the calculated quadrupole moments and $E2$, $E3$ transition rates with the experimental ones [18,36–39]. The agreement is very good, the only discrepancy regarding the $B(E2; 2^+_1 \rightarrow 0^+_1)$ in ^{210}Po. It should be mentioned, however, that the experimental value was obtained by comparing the cross section $\sigma(2^+, ^{210}\text{Po})$ measured in a ^{210}Po study by inelastic scattering of deuterons with the corresponding one for ^{206}Pb [40]. As far as the quadrupole moments are concerned, four out of the five calculated values are within the error bars and the observed signs, when measured, are correctly reproduced. It is worth noting that our results do not differ significantly from those obtained using an effective proton charge $e_p^{\text{eff}} = 1.5e$, which is consistent with the values adopted by other authors [16,17].

As regards the $B(E3)$'s, they are all underestimated by our calculations. It is well known that enhanced $E3$ transitions in nuclei in the lead region can be taken as a signature of mixing of the 3^- core excitation into the involved levels [41]. We should note, however, that whereas our calculations

TABLE VI. Calculated and experimental quadrupole moments (in e b).

Nucleus	J^π	Q	
		Calc.	Expt.
^{210}Po	8_1^+	-0.588	-0.552 ± 0.020
	11_1^-	-0.92	-0.86 ± 0.11
^{211}At	$(\frac{21}{2}^-)_1$	-0.54	$\pm0.53\pm0.05$
	$(\frac{29}{2}^+)_1$	-1.07	$\pm1.01\pm0.19$
^{212}Rn	8_1^+	-0.29	$(-)0.17\pm0.02$

fail to reproduce the $B(E3)$ values, a good description of the states involved in such transitions is obtained for the excitation energies as well as for the other electromagnetic properties. Thus, these states are likely to contain very small components of octupole excitation which, however, are sufficient to largely enhance the $E3$ transition rates. In particular, the $E3$ transitions in ^{211}At and ^{212}Rn, and the $11_1^- \rightarrow 8_2^+$ transition in ^{210}Po correspond to the single-particle transition $i_{13/2} \rightarrow f_{7/2}$, which is expected to be very fast owing to the coupling between the $f_{7/2}$ orbital and the 3^- collective state [42]. The $11_1^- \rightarrow 8_1^+$ transition in ^{210}Po is instead of the type $i_{13/2} \rightarrow h_{9/2}$ and is slowed down by spin flip.

IV. DISCUSSION AND CONCLUSIONS

In this work, we have performed shell-model calculations for the $N=126$ isotones ^{210}Po, ^{211}At, and ^{212}Rn, employing an effective interaction derived from the Bonn-A nucleon-nucleon potential by means of a G-matrix folded-diagram method. As for the single-proton energies, we have taken them from the experimental spectrum of ^{209}Bi. It should be stressed that, since we have also derived in a microscopic way the effective operators needed for the calculation of electromagnetic observables, no use has been made of any adjustable parameter.

These calculations, as well as the previous ones on neutron hole Pb isotopes [14,21], are the first in the ^{208}Pb region where a modern realistic interaction has been used. As already mentioned in the Introduction, the first attempt to employ in this region effective interactions derived from the free nucleon-nucleon potential dates back to the early 1970s [17]. In that work, however, the Hamada-Johnston NN potential was used and only the $3p$-$1h$ core-polarization diagram (the so-called bubble) was included in the calculation of the effective interaction. It should also be noted that to obtain good agreement with experiment for the $^{204-206}$Pb isotopes, the bubble was multiplied by the empirical factor 0.75.

As regards our calculations, we have obtained a very good

TABLE VII. Calculated and experimental reduced transition probabilities (in W.u.).

Nucleus	Transition	$J_i^\pi \rightarrow J_f^\pi$	Reduced transition probabilities	
			Calc.	Expt.
^{210}Po	$E2$	$2_1^+ \rightarrow 0_1^+$	3.55	0.56 ± 0.12
	$E2$	$4_1^+ \rightarrow 2_1^+$	4.46	4.53 ± 0.15
	$E2$	$6_1^+ \rightarrow 4_1^+$	3.07	3.00 ± 0.12
	$E2$	$8_1^+ \rightarrow 6_1^+$	1.25	1.10 ± 0.05
	$E3$	$11_1^- \rightarrow 8_2^+$	6.1	19.7 ± 1.1
	$E3$	$11_1^- \rightarrow 8_1^+$	0.55	3.71 ± 0.10
^{211}At	$E2$	$(\frac{3}{2}^-)_1 \rightarrow (\frac{5}{2}^-)_1$	10.1	12.5 ± 1.4
	$E2$	$(\frac{3}{2}^-)_1 \rightarrow (\frac{7}{2}^-)_2$	1.67	1.77 ± 0.17
	$E2$	$(\frac{3}{2}^-)_1 \rightarrow (\frac{7}{2}^-)_1$	0.15	0.39 ± 0.04
	$E2$	$(\frac{15}{2}^-)_1 \rightarrow (\frac{11}{2}^-)_1$	2.3	1.3 ± 0.3
	$E2$	$(\frac{21}{2}^-)_1 \rightarrow (\frac{17}{2}^-)_1$	2.60	2.51 ± 0.05
	$E2$	$(\frac{29}{2}^+)_1 \rightarrow (\frac{25}{2}^+)_1$	1.6	1.8 ± 0.5
	$M1$	$(\frac{3}{2}^-)_1 \rightarrow (\frac{5}{2}^-)_1$	8×10^{-7}	$1.4\times10^{-4}\pm0.4\times10^{-4}$
	$M1$	$(\frac{15}{2}^-)_1 \rightarrow (\frac{13}{2}^-)_1$	8×10^{-7}	$0.7\times10^{-4}\pm0.2\times10^{-4}$
	$E3$	$(\frac{29}{2}^+)_1 \rightarrow (\frac{23}{2}^-)_1$	6.3	20.1 ± 1.8
^{212}Rn	$E2$	$4_1^+ \rightarrow 2_1^+$	1.42	1.04 ± 0.04
	$E2$	$6_1^+ \rightarrow 4_1^+$	0.73	0.40 ± 0.05
	$E2$	$8_1^+ \rightarrow 6_1^+$	0.252	0.115 ± 0.006
	$E2$	$12_1^+ \rightarrow 10_1^+$	3.6	4.4 ± 0.2
	$E2$	$14_1^+ \rightarrow 12_1^+$	0.008	0.032 ± 0.008
	$E2$	$14_1^+ \rightarrow 12_2^+$	3.4	3.6 ± 0.5
	$E2$	$17_1^- \rightarrow 15_1^-$	2.9	3.0 ± 1.6
	$E3$	$17_1^- \rightarrow 14_1^+$	6	16 ± 6

description of both $N=126$ isotones and Pb isotopes in a truly microscopic way. It cannot be said, however, that our agreement with experiment is much better than that obtained in Ref. [17]. In this connection, we found it worthwhile to calculate the complete energy spectrum of ^{210}Po up to 5 MeV making use of the KH effective interaction. It turned out that the σ value relative to the 37 levels considered in Sec. III A is 116 keV, namely, only about 30 keV larger than our value. On the other hand, it should be mentioned that a comparison between the results of the two calculations evidences more substantial differences. More precisely, the calculation with the KH interaction predicts some levels to lie 300–400 keV above those obtained with our effective interaction. We do not feel, however, that a detailed comparison between the two kinds of calculations is very meaningful. We consider as the main achievement of our studies of nuclei around ^{208}Pb to have shown that effective interactions derived from the Bonn-A potential by means of a *G*-matrix folded-diagram approach lead to a quite accurate description of these nuclei. This outcome acquires more relevance when considered along with the results of our studies on nuclei with few valence particles or holes in the region of doubly magic ^{100}Sn and ^{132}Sn [1–3,5]. In fact, the remarkable overall agreement with experiment obtained in all cases considered leads to the conclusion that the new generation of realistic effective interactions is quite adequate for nuclear structure calculations.

Actually, being focused on identical particle systems, our studies provide a stringent test of the isospin $T=1$ matrix elements of the effective interaction. A test of the $T=0$ matrix elements is of course equally important. In this connection, it may be mentioned that in earlier works [12] it turned out that not enough attraction was provided by the calculated matrix elements of the $T=0$ effective interaction, which has a stronger dependence on the tensor force strength than the $T=1$ interaction. We should point out, however, that in a recent study [4] of the doubly odd nucleus ^{132}Sb we have obtained results which are as good as those regarding like nucleon systems. Along the same lines we are currently studying other nuclei with both neutrons and protons outside closed shells.

A main question relevant to microscopic nuclear structure calculations is the extent to which they depend on the *NN* potential used as input. We are currently trying to explore this problem. Preliminary calculations indicate that different *NN* potentials produce somewhat different nuclear structure results [1,43]. In particular, it has turned out that the best agreement with experiment is produced by the Bonn-A potential.

In conclusion, at the present stage of our investigation of the role of realistic effective interactions in complex nuclei, it is our belief that a truly microscopic description of nuclear structure properties is now within reach.

ACKNOWLEDGMENTS

This work was supported in part by the Italian Ministero dell'Università e della Ricerca Scientifica e Tecnologica (MURST) and by U.S. DOE Grant No. DE-FG02-88ER40388.

[1] F. Andreozzi, L. Coraggio, A. Covello, A. Gargano, T. T. S. Kuo, Z. B. Li, and A. Porrino, Phys. Rev. C **54**, 1636 (1996).
[2] F. Andreozzi, L. Coraggio, A. Covello, A. Gargano, T. T. S. Kuo, and A. Porrino, Phys. Rev. C **56**, R16 (1997).
[3] A. Covello, L. Coraggio, and A. Gargano, Nuovo Cimento A **111**, 803 (1998).
[4] F. Andreozzi, L. Coraggio, A. Covello, A. Gargano, T. T. S. Kuo, and A. Porrino, Phys. Rev. C **59**, 746 (1999).
[5] A. Covello, F. Andreozzi, L. Coraggio, A. Gargano, and A. Porrino, in *Highlights of Modern Nuclear Structure*, Proceedings of the Sixth International Spring Seminar on Nuclear Physics, S. Agata sui due Golfi, 1998, edited by A. Covello (World Scientific, Singapore, 1999), p. 129.
[6] R. Machleidt, K. Holinde, and Ch. Elster, Phys. Rep. **149**, 1 (1987).
[7] T. T. S. Kuo and G. E. Brown, Nucl. Phys. **85**, 40 (1966).
[8] T. Hamada and I. D. Johnston, Nucl. Phys. **34**, 382 (1962).
[9] G. H. Herling and T. T. S. Kuo, Nucl. Phys. **A181**, 113 (1970).
[10] R. Machleidt and G. Q. Li, Phys. Rep. **241**, 5 (1994).
[11] R. Machleidt, in *Highlights of Modern Nuclear Structure* [5], p. 57.
[12] M. F. Jiang, R. Machleidt, D. B. Stout, and T. T. S. Kuo, Phys. Rev. C **46**, 910 (1992).
[13] T. T. S. Kuo, in *New Perspectives in Nuclear Stucture*, Proceedings of the Fifth International Spring Seminar on Nuclear Physics, Ravello, 1995, edited by A. Covello (World Scientific, Singapore, 1996), p. 131.
[14] L. Coraggio, A. Covello, A. Gargano, N. Itaco, and T. T. S. Kuo, Phys. Rev. C **58**, 3346 (1998).
[15] C. W. Ma and W. W. True, Phys. Rev. C **8**, 2313 (1972), and references therein.
[16] D. Zwarts and P. W. M. Glaudemans, Z. Phys. A **320**, 487 (1985), and references therein.
[17] J. B. McGrory and T. T. S. Kuo, Nucl. Phys. **A247**, 283 (1975).
[18] Data extracted using the NNDC On-Line Data Service from the ENSDF database, file revised as of June 25, 1999, M. R. Bhat, *Evaluated Nuclear Structure Data File (ENSDF), Nuclear Data for Science and Technology*, edited by S. M. Qaim (Springer-Verlag, Berlin, Germany, 1992), p. 817.
[19] E. M. Krenciglowa, C. L. Kung, T. T. S. Kuo, and E. Osnes, Ann. Phys. (N.Y.) **101**, 154 (1976).
[20] S. F. Tsai and T. T. S. Kuo, Phys. Lett. **39B**, 427 (1972).
[21] A. Covello, L. Coraggio, A. Gargano, and N. Itaco, Acta Phys. Pol. B **30**, 715 (1999).
[22] J. Shurpin, T. T. S. Kuo, and D. Strottman, Nucl. Phys. **A408**, 310 (1983).
[23] T. T. S. Kuo and E. M. Krenciglowa, Nucl. Phys. **A342**, 454 (1980).
[24] K. Suzuki and S. Y. Lee, Prog. Theor. Phys. **64**, 2091 (1980).
[25] B. A. Brown, A. Etchegoyen, and W. D. M. Rae, The computer code OXBASH, MSU-NSCL, Report No. 524.
[26] H. A. Mavromatis, L. Zamick, and G. E. Brown, Nucl. Phys. **80**, 545 (1966).

[27] E. M. Krenciglowa and T. T. S. Kuo, Nucl. Phys. **A240**, 195 (1975).
[28] H. Hyuga and A. Arima, J. Phys. Soc. Jpn. Suppl. **34**, 538 (1973).
[29] I. S. Towner, F. C. Khanna, and O. Häusser, Nucl. Phys. **A277**, 285 (1977).
[30] G. Audi and A. H. Wapstra, Nucl. Phys. **A565**, 1 (1993).
[31] L. G. Mann, K. H. Maier, A. Aprahamian, J. A. Becker, D. J. Decman, E. A. Henry, R. A. Meyer, N. Roy, W. Stöffl, and G. L. Struble, Phys. Rev. C **38**, 74 (1988).
[32] H. Klein, I. Wiedenhöver, H. Tiesler, H. Meise, A. Fitzler, A. Dewald, H. G. Thomas, D. Weisshaar, and P. von Brentano, Eur. Phys. J. A **4**, 221 (1999).
[33] We define $\sigma=\{(1/N_d)\Sigma_i[E_{\rm exp}(i)-E_{\rm calc}(i)]^2\}^{1/2}$, where N_d is the number of data.
[34] R. Groleau, W. A. Landford, and R. Kouzes, Phys. Rev. C **22**, 440 (1980).
[35] G. Astner, Phys. Scr. **5**, 31 (1972).
[36] P. Raghavan, At. Data Nucl. Data Tables **42**, 189 (1989).
[37] S. Bayer, A. P. Byrne, and G. D. Dracoulis, Nucl. Phys. **A591**, 104 (1995).
[38] A. E. Stuchbery, A. P. Byrne, G. D. Dracoulis, B. Fabricious, and T. Kibédi, Nucl. Phys. **A555**, 355 (1993).
[39] J. A. Becker *et al.*, Nucl. Phys. **A522**, 483 (1991).
[40] C. Ellegaard, P. D. Barnes, R. Eisenstein, E. Romberg, T. S. Bhatia, and T. R. Canada, Nucl. Phys. **A206**, 83 (1973).
[41] I. Bergström and B. Fant, Phys. Scr. **31**, 26 (1985).
[42] A. Bohr and B. R. Mottelson, *Nuclear Structure*, Vol. II (Benjamin, New York, 1975), p. 566.
[43] A. Covello, L. Coraggio, A. Gargano, N. Itaco, and T. T. S. Kuo, *Proceedings of the Nuclear Structure 98 Conference*, Gatlinburg, Tennessee, 1998, edited by C. Baktash (AIP, New York, 1999).